Journal of Hazardous Materials 198 (2011) 269–274

Contents lists available at SciVerse ScienceDirect

Journal of Hazardous Materials

journal homepage: www.elsevier.com/locate/jhazmat

Effect of self-glazing on reducing the radioactivity levels of red mud based ceramic materials☆

Shuo Qin, Bolin Wu*

College of Material Science and Engineering, Guilin University of Technology, Guilin, Guangxi 541004, PR China

ARTICLE INFO

Article history:
Received 29 March 2011
Received in revised form 10 October 2011
Accepted 13 October 2011
Available online 18 October 2011

Keywords:
Red mud
Self-glazing
Radioactivity levels
Reduction

ABSTRACT

Self-glazing red mud based ceramic materials (RMCM) were produced by normal pressure sintering process using the main raw materials of red mud. The properties of the RMCM samples were investigated by the measurements of mechanical properties, radiation measurement, X-ray diffraction (XRD) and scanning electron microscopy (SEM). The results show that the self-glazing RMCM have good mechanical properties (water absorption and apparent porosity approached zero; bulk density, 2.94 g/cm^3; compressive strength, 78.12 MPa). The radiation level has clear change regularity that the radioactivity levels of red mud (6360 Bq) is obvious declined, and can be reduced to that of the natural radioactive background of Guilin Karst landform, China (3600 Bq). It will not only consume large quantities of red mud, but also decrease the production cost of self-glazing RMCM. And the statement of this paper will offer effective ways to reduce the radioactivity level of red mud.

1. Introduction

"Bauxite residue", also known as "red mud", is the by-product of the digestion of bauxite ores with caustic soda in high pressure autoclaves according to the Bayer process, in order to produce alumina [1]. It is a complex material whose mineralogical and chemical composition vary widely depending upon the source of bauxite ores and the technological process parameters [2]. A chemical analysis would indicate that red mud contains silica, aluminum, iron, calcium, titanium, as well as an array of minor constituents, namely, Cr, Cu, K, Mn, Na, Ni, Sc, Th, U, V, Zn, etc. The variation in chemical composition between different red mud worldwide is high [3]. This residue is disposed as a mud disposal possessing a solid concentration in the range of 10–30%, potential of hydrogen in the range of 13 and high ionic strength [4]. Consequently, red mud with the characteristics of high alkalinity [5] and high level radioactivity [6] having been accumulated in the dam construction and storage yard [7], is viewed as a corrosively hazardous substance requiring carefully handling. This caustic material is often contained in constructed storage facility to minimize its adverse impacts on the human beings and environments [8].

Therefore, from the viewpoint of waste disposal, how to recycle the red mud and improve the ratio of recycled resources have become very important environmental project on subjects [9]. In recent years, voluminous research and development work for the comprehensive utilizations of red mud have been put into practice all over the world, but to date very few techno-economical solutions have been found out [10]. Studies on the utilization of red mud for making efficient and low-priced building materials namely ordinary Portland cement [11], clay-based ceramics [12], bricks [13], and glass-ceramics [14] have been reported. However, more and more precedence is being given to limiting the radiological dose of building materials to the population these days. Somlai et al. [15] had measured ^{226}Ra and ^{232}Th activity concentrations in Hungarian bauxite, red mud and clay samples and the result is similar with the levels for such raw materials mentioned in international literature. Therefore for the production of building materials an even stricter limit needs to be determined when both bauxite and red mud are used. The application of radiation protection technology is increasing day by day all over the world [16]. Amritphale et al. [10] had reported that they could prepare the X-ray radiation-shielding materials from red mud and fly ash [17].

Based on previous work in our laboratory, we found that a glaze layer forms on the red mud based ceramic surface automatically when red mud is sintering [18]. Since the release glazed ceramics and does not require preparation of glazes and glazing techniques, the sintering process of self-glazed surface of the green body formation. This is so-called self-glazing phenomenon that can give significant brightness and high aesthetic quality [19]. According to a well-researched of the origin, Egyptian paste (also known as Egyptian faience) is the first material of self-glazing ceramic body

☆ This work was supported by National Natural Science Foundation of China (No. 50972028), Science and Technology Department of Guangxi Zhuang Autonomous Region of China (No. 0630006-5).

* Corresponding author.
E-mail address: wubolin3211@gmail.com (B. Wu).

0304-3894/$ – see front matter © 2011 Elsevier B.V. All rights reserved.
doi:10.1016/j.jhazmat.2011.10.039

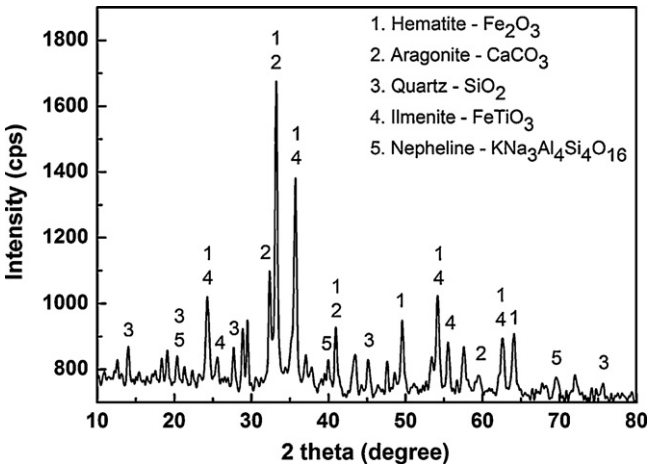

Fig. 1. The main mineralogical phases of red mud.

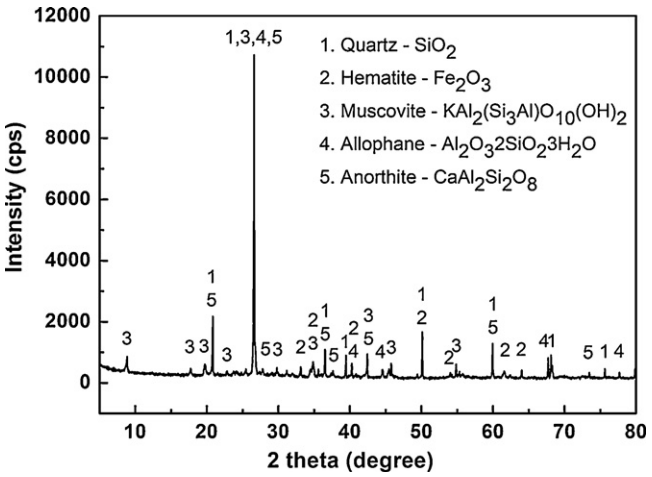

Fig. 2. The main mineralogical phases of red sandstone.

that no further glaze will be needed for the Egyptian paste piece to fire with a glossy glaze surface [20]. Merkin et al. [21] have mixed the acid volcanic glasses, obsidians, pechsteins, perlite raw materials waste and volcanic minerals, to produce self-glazing ceramic tiles. Griggs et al. [22] have restored the surface of dental porcelain using a self-glazing technique that may reduce the extent of damage caused by grinding and prevent bacterial adhesion. In view of the above discussions and for five years' exploration of the comprehensive utilization of red mud in our laboratory, the high Si/Al ratio compositions in red mud can react with oxides of alkaline metal, silicon and heavy-metal, which together with barium feldspar [23] may reduce the radiation levels of red mud effectively. In this study, the red mud based ceramic materials (RMCM) were prepared, and of which the physical properties, radioactivity levels, phase analysis, microstructure and self-glazing mechanism have been investigated.

2. Experimental

2.1. Raw materials and chemicals

The objective of the experiment is to reduce the radioactivity levels of red mud based ceramic materials. Red mud contains large amounts of Fe_2O_3, Al_2O_3 and CaO, but little SiO_2. However, red sandstone and ball clay contain large amounts of SiO_2, which can sinter with red mud to obtain ceramics. The red mud supplied by Pingguo Aluminum Company (Guangxi, China), the red sandstone obtained from Dayao Mountain (Guangxi, China) and the ball clay obtained from Weiluo (Guangxi, China) were milled into powder with particles size lower than 100 μm, respectively. The chemical composition of the raw materials is presented in Table 1, and the mineralogical phases of red mud, red sandstone and ball clay were determined by XRD analysis as shown in Figs. 1–3, respectively.

The barium carbonate and red lead chemicals are heavy-metal compounds, which can shield the radiation effectively. The barium carbonate chemicals of Technical Grade were from Silian Chemical Plant (Shanghai, China) and dried at 105 °C for 6 h. The red lead (lead (II, IV) oxide, red) of AR Grade was produced by Nanhua Chemical Plant (Hunan, China). Magnesium oxide of AR Grade was from Beifang Tianyi Chemical Reagent Plant (Tianjin, China), and calcium oxide of AR Grade was from Xilong Chemical Plant (Shantou, China).

2.2. Experimental procedure

In the experiments, certain amount of red mud, red sandstone and ball clay was ball milled in water medium for 24 h, respectively. Then the raw material mixtures were prepared by homogenizing red mud, red sandstone and ball clay at certain mixture ratio with barium carbonate, red lead and oxides of magnesium, calcium additions. After homogenization, the mixture was dried in an air oven at 105 °C, the powder mix was mixed with 1 wt% water and compressed into circular samples of 50 mm diameter and 3–4 mm thickness by uniaxial pressing under a pressure of 10 MPa. Then the green bodies were sintered in a box type electrical resistance furnace. The sintering condition was programmed as follows: heating from ambient temperature to 100 °C at a heating rate of 5 °C/min, holding for 30 min at 100 °C; heating to 700 °C at rate of 4 °C, holding for 60 min at 700 °C; and then sintering at 700–1100 °C at rate of 3 °C, holding for 60 min at the sintering point; and finally cooling of samples in the furnace itself down to ambient temperature.

2.3. Testing conditions

2.3.1. Determination of the properties

Water absorption, bulk density and apparent porosity of the sintered samples were determined respectively in accordance with Chinese National Standard GB/T 3810.3-2006 [24]. The water absorption (Wa, %), bulk density (Db, g/cm^3) and

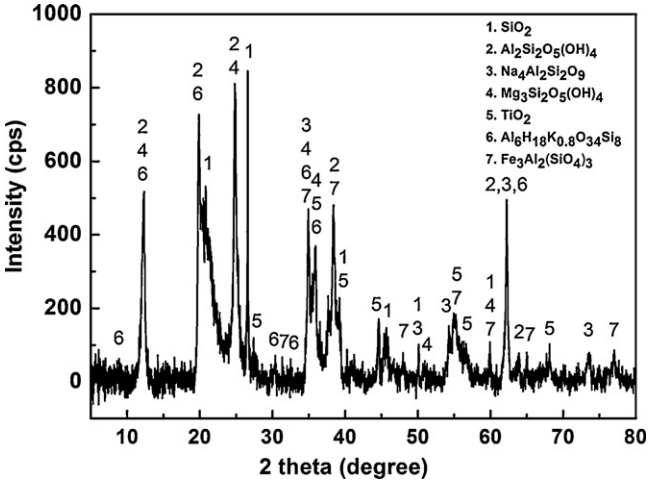

Fig. 3. The main mineralogical phases of ball clay.

Table 1
Chemical compositions (wt%) of the raw materials (LOI, loss on ignition at 1050 °C).

Constituent	Fe_2O_3	Al_2O_3	SiO_2	CaO	MgO	TiO_2	K_2O	Na_2O	LOI	Other
Red mud	31.26	18.49	8.35	18.05	0.72	6.18	0.20	3.23	9.80	3.72
Red sandstone	4.87	13.94	60.82	8.09	–	–	–	–	2.66	9.62
Ball clay	0.67	36.56	45.37	0.21	0.65	1.58	0.48	0.04	13.93	0.51

apparent porosity (Pa, %) were calculated basing on the formulas $Wa = (M3 - M1)/M1 \times 100\%$, $Db = (M1 \times DL)/(M3 - M2)$ and $Pa = (M3 - M1)/(M3 - M2) \times 100\%$, respectively, where $M1$ is the weight of dry sample measured in the air (g), $M2$ the weight of saturated sample measured in the soak solution (g), $M3$ the weight of saturated sample measured in the air (g) and DL is the density of the soak solution (g/cm^3).

The linear shrinkage measurement of sintered samples was performed according to Chinese Light Industry Standard QB/T 1548-1992 [25]. The formula for calculating the linear shrinkage (Y, %) is $Y = (L1 - L2)/L1 \times 100\%$, where $L1$ is the average diameter of dry green body (mm) and $L2$ is the average diameter of sintered sample (mm).

The sintered ceramic samples of cylinder size Φ20 mm × 20 mm were evaluated for their compressive strength following Chinese National Standard GB/T 4740-1999 [26]. The loading speed was 1 mm/min. Compressive strength (σ_e, MPa) was calculated basing on the formula $\sigma_e = 4P/\pi D^2$, where P is the maximum load of sample fracture under pressure (N), π the circumference ratio and D is the diameter of the tested sample (mm).

2.3.2. Measurement of radioactivity levels

The radioactivity levels of raw materials, chemicals, the natural radioactive background, and testing samples were measured using a radiation detector (Inspector Alert), model No. Inspector of INSPECTOR, U.S.A. The number of counts detected by the Inspector Alert varies from reading to reading due to the random nature of radioactivity. A reading is expressed more accurately as an average over time, and the average is more accurate over a longer time period. Therefore, radiation measurement was operated in Total/Timer mode to take a total count for a timed period of three minutes obtaining three-minute average in this study. The SI unit Becquerel (Bq) was used in this paper which is calculated by the relational expression 1 Total/Timer = 1 CPM = 60 Bq.

2.3.3. X-ray powder diffraction analysis

The X-ray powder diffraction study of the sintered samples was carried out using an X-ray diffractometer (XRD) (Cu Kα1, 1.54060 Å, Model No. X'Pert PRO, PANalytical B.V, Almelo, Holland) with voltage 40 kV, current 40 mA. X-ray patterns were taking by measuring 2θ from 5° to 80°, at a step size of 0.02° and a dwell time of 5 s per step. The resulting powder diffraction patterns were analyzed utilizing a software package program.

Table 2
Properties of the RMCM.

Tests	Results	Criterion of common ceramics
Water absorption (%)	0.004	≤1.0
Bulk density (g/cm^3)	2.94	≥2.5
Apparent porosity (%)	0.012	≤15.0
Linear shrinkage (%)	12.26	≤10.0
Compressive strength (MPa)	78.12	≥30.0

2.3.4. The scanning electron microscope analysis

The fracture surface microstructure observation of the sintered samples was investigated using a scanning electron microscope (SEM), model No. JSM-6380LV of JEOL Ltd., Tokyo, Japan. The samples were coated with carbon prior to examination. The microstructure of the samples was examined in detail using SEM and the micrographs were taken.

3. Results and discussion

3.1. Properties of the self-glazing ceramic materials

The photograph of RMCM specimen is shown in Fig. 4. As shown in Fig. 4, RMCM specimen of Φ20 mm × 3 mm was prepared by molding and sintering. It is apparent that the ceramics surface is shiny and smooth, and the glaze layer is full (cf. Fig. 4A). The red mud based ceramic green body composed of oxides of alkaline metal, silicon and heavy-metal that, when sintered, produces its own glaze coating. No further glaze will be needed for the green body to fire with a glossy glaze surface. The specimen does not appear to have quality problems, such as dehiscing, warping and transmogrifying (cf. Fig. 4B).

The results of properties tests are summarized in Table 2. According to the test results, both water absorption and apparent porosity of the self-glazing ceramic materials decreased and approached zero very well within the red mud self-glazing system. The bulk density of the ceramic materials was about 15% higher than that of common ceramics criterion. The compressive strength

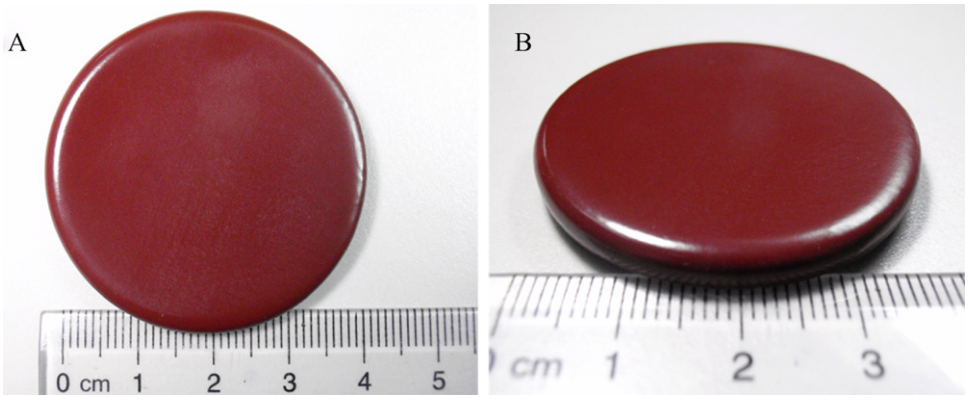

Fig. 4. Photograph of RMCM specimen.

Fig. 5. Photograph of RMSS specimen.

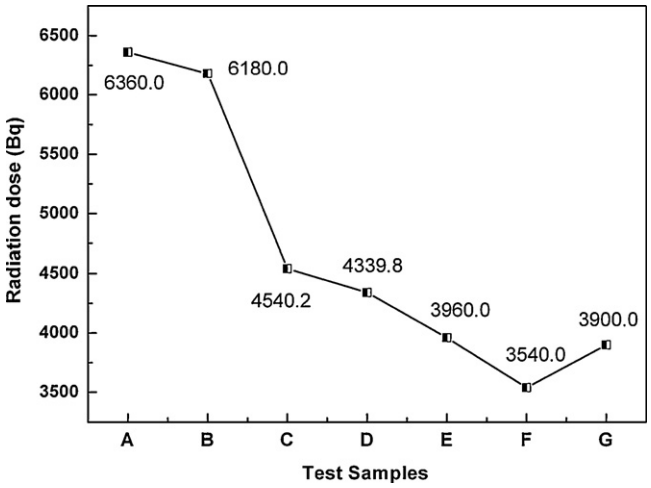

Fig. 6. Radioactivity levels of test samples. (A) Red mud untreated; (B) red mud milled for 24 h and dried at 105 °C for 8 h; (C) the green body contained heavy-metal oxide; (D) the RMCM contained no heavy-metal oxide obtained at 1000 °C, 1 h; (E) under-burnt RMCM contained heavy-metal oxide obtained at 950 °C, 1 h; (F) self-glazing RMCM contained heavy-metal oxide obtained at 1050 °C, 1 h; (G) over-burnt RMCM contained heavy-metal oxide obtained at 1150 °C, 1 h).

of the ceramic materials has reached value of 78.12 MPa, which was much higher than that of the requirement of structural materials provide in Chinese National Standard GB 5101-2003 [27]. The inorganic high-temperature reactions help to accelerate the strength development of RMCM at high-temperature stages of sintering. However, the linear shrinkage of RMCM did not meet the requirement of common ceramics criterion. In consideration of the high linear shrinkage in a part of RMCM, we had developed another spherical RMCM, so-called red mud based sintering sand (RMSS). The photograph of RMSS specimen is shown in Fig. 5, it can be seen that the RMSS also produce their own glaze coating and the surfaces are shiny.

It can be inferred from the properties that it is feasible to use red mud and other oxides of alkaline metal, silicon and heavy-metal to produce self-glazing RMCM and RMSS. Possessing important environmental and economic significances, the produced self-glazing RMCM and RMSS will not only consume large quantities of red mud, but also decrease the production cost of RMCM and RMSS.

3.2. Radioactivity levels of raw materials and the natural radioactive background

The radioactivity levels of raw materials, chemicals and the natural radioactive background were measured by the Inspector Alert. The number of counts detected by the Inspector Alert varies from reading to reading due to the random nature of radioactivity. A reading is expressed more accurately as an average over time, and the average is more accurate over a longer time period. In order to interpret the readings getting on the Inspector Alert accurately, the natural radioactive background level of the area where the experiment was carried out should be established. The radioactivity levels of raw materials, chemicals and the natural radioactive background level are listed in Table 3.

Table 3 shows that the radioactivity levels of red mud (6360 Bq) is about 76.6 percent higher than that of Guilin's background level (3600 Bq). Guilin is the most typical and rare example of Karst Topography in terms of its scale and uniqueness. In geographic terms, Karst Topography is a landscape shaped by the chemical denudation of a layer, suffusion and erosion of water, or layers of soluble bedrock for hundreds of million years, usually carbonate rock such as limestone or dolomite [28]. Therefore, the natural radiation level of Karst area is considerable low [29–31]. If the radioactivity levels of RMCM can be reduced to that of the natural radioactive background of Guilin Area, the materials can be used in some areas.

3.3. The regularity and mechanism of reducing the radioactivity levels of RMCM

The results of radiation measurement of red mud, green body and sintered samples are given in Fig. 6. According to measured data of the test samples, in order of raw material (red mud) – ball milling – green body – sintered samples (under-burnt) – self-glazing samples (be rich in glass phases) – over-burnt samples (high porosity), the radiation level has clear change law: the radioactivity levels of red mud is obvious declined, and can be reduced to that of the natural radioactive background of Guilin Area, China.

Milled for a period of time, the radioactivity levels of red mud can be reduced from 6360 Bq (Sample A) to 6180 Bq (Sample B), because fine particles have excellent adsorption to alpha and beta particles, and the fine structure has superiority of blocking radiation to the emission of alpha, beta and gamma rays. By adding a certain amount of heavy-metal compounds in materials and compressing into green body, the radiation level can be evidently reduced to 4540.2 Bq (Sample C). According to the Bethe–Bloch formula of classical quantum theory, energy-loss rate is directly proportional to atomic number and number density of atoms in matter [32,33]; that is, materials with high atomic number and high density which have excellent stopping power to radiation particles, and the action of fine structure is more conspicuous in radiation-shielding. The green bodies were calcined in air ambience to obtain sintered samples with high compactness and high atom density. The radioactivity levels of sample containing heavy metals (Sample E) are lower than that of sample containing no heavy metals (Sample D). Within the pale of sintering temperature, a rise in sintering temperature resulted in a rapid increase in the glass phases of sample (Sample F), and the radiation level of Sample F can be reduced to 3540 Bq to meet the level of the natural radioactive background of Guilin Area, China. But, with the increasing of sintering temperature, the sample undergoes over-burnt progress resulting in high porosity, of which the radioactivity level increase a little (Sample G).

The XRD patterns of the self-glazing RMCM (Sample F) are presented in Fig. 7, and the respective phases identified are given in Table 4. It can be seen that the main crystal phase ($CaAl_4Fe_8O_{19}$, hematite, quartz and calcium silicate) and minor crystal phase (ilmenite and perovskite) appeared in the sample obtained during

Table 3
Radioactivity levels of raw materials, chemicals and the natural radioactive background.

Designation	Red mud	Red sandstone	$BaCO_3$	Red lead	CaO	MgO	Natural radioactive background[a]
Radioactivity levels (Bq)	6360.0	3940.2	3840.0	3840.0	3799.8	4159.8	3600.0

[a] The natural radioactive background level of Guilin Area, China.

Table 4
The main mineralogical phases present in the self-glazing RMCM.

Peak number	Mineral name	Chemical formula	Reference code	Crystal system
1	Calcium aluminum iron oxide	$CaAl_4Fe_8O_{19}$	00-049-1586	Hexagonal
2	Hematite	Fe_2O_3	01-089-0598	Rhombohedral
3	Quartz	SiO_2	01-078-1254	Hexagonal
4	Calcium silicate	$Ca_2(SiO_4)$	01-086-0401	Hexagonal
5	Ilmenite	$FeTiO_3$	01-075-1212	Rhombohedral
6	Perovskite	$CaTiO_3$	01-082-0229	Orthorhombic
7	Barium silicate	$BaSiO_3$	01-070-2112	Orthorhombic

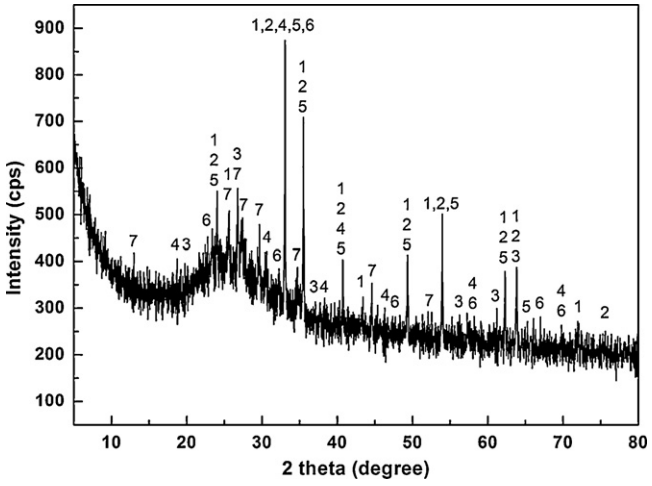

Fig. 7. XRD patterns of the self-glazing RMCM.

sintering. Raw materials component such as CaO, Al_2O_3, SiO_2 and BaO dissolved to construct the CaO–Al_2O_3–SiO_2 system and BaO–Al_2O_3–SiO_2 system glass phases at high sintering temperature to obtain long-term durability and high strength of vitrification samples which have excellent radiopaque power to a variety of radioactive elements and radioisotopes.

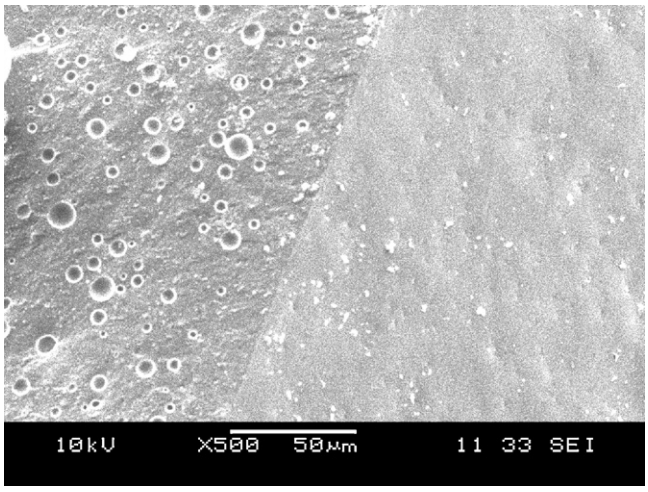

Fig. 8. SEM micrograph of fracture surface of the self-glazing RMCM.

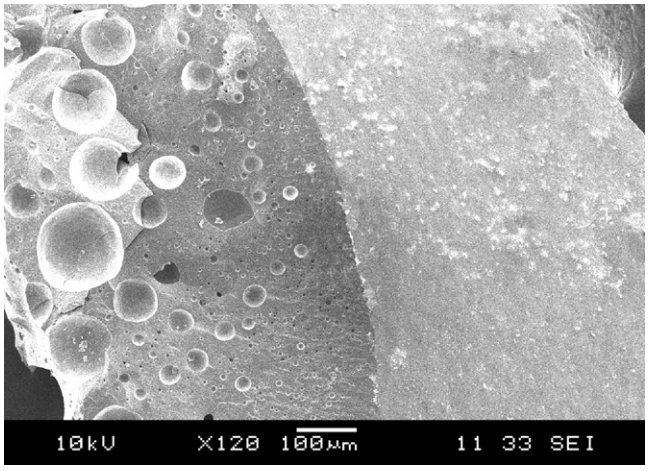

Fig. 9. SEM micrograph of fracture surface of the over-burnt RMCM.

The scanning electron microphotograph exhibiting the fracture surface microstructure of the self-glazing RMCM is given in Fig. 8. The micrograph shows that large quantities of small pores observed inside the ceramics (cf. the left area of Fig. 8). The pores within the green body are hindered by the melt on interface between the green body and high viscosity melt with the rising of firing temperature. During the cooling process, the high temperature melt is cooled to form glass phases, and due to the surface tension of the melt, the formation of spherical pores as shown in Fig. 8 are created. Therefore, the formation of spherical pores indicates the occurrences of the self-glazing phenomenon.

Fig. 9 presents the microstructure of the over-burnt RMCM. Due to large quantities of big pores within the RMCM, the radiopaque power decrease with the increasing of radiating area. Therefore, the radioactivity level of Sample G increases a little contrast to the self-glazing RMCM.

4. Conclusions

Based on the results of the present investigation, the following conclusions can be drawn:

(1) The red mud based ceramic green body composed of oxides of alkaline metal, silicon and heavy-metal produces can undergo a phenomenon so-called self-glazing when sintered. No further glaze will be needed for the green body to fire with a glossy glaze surface.

(2) In order of raw material (red mud) – ball milling – green body – sintered samples (under-burnt) – self-glazing samples (be rich in glass phases) – over-burnt samples (high porosity), the radiation level has clear change law: the radioactivity levels of red mud (6360 Bq) are obvious declined, and can be reduced to that of the natural radioactive background of Guilin Area, China (3600 Bq).
(3) The XRD and SEM analyses have revealed that a considerable content of glass phases created in the ceramic materials during the sintering process. The radioactivity levels of RMCM can be reduced prominently by the self-glazing.
(4) Possessing important environmental and economic significances, it will not only consume large quantities of red mud, but also decrease the production cost of RMCM and RMSS.

Acknowledgements

We gratefully acknowledge Prof. WU Bolin, Dr. Ou Jun, Dr. HU Changzheng and Senior Engineer ZHU Wenfeng of Guilin University of Technology, for their kind help in experimental instructions and radioactivity levels test, mechanical properties test, XRD test and SEM test, respectively.

References

[1] Y. Ma, C. Lin, Y. Jiang, W. Lu, C. Si, Y. Liu, Competitive removal of water-borne copper, zinc and cadmium by a $CaCO_3$-dominated red mud, J. Hazard. Mater. 172 (2009) 1288–1296.
[2] M. Singh, S.N. Upadhayay, P.M. Prasad, Preparation of special cements from red mud, Waste Manage. 16 (1996) 665–670.
[3] A.R. Hind, S.K. Bhargava, S.C. Grocott, The surface chemistry of Bayer process solids: a review, Colloids Surf. A 146 (1999) 359–374.
[4] Characteristics, Red Mud Red Mud Project. http://www.redmud.org/Characteristics.html.
[5] M. Johnston, M.W. Clark, P. McMahon, N. Ward, Alkalinity conversion of bauxite refinery residues by neutralization, J. Hazard. Mater. 182 (2010) 710–715.
[6] A. Akinci, R. Artir, Characterization of trace elements and radionuclides and their risk assessment in red mud, Mater. Charact. 59 (2008) 417–421.
[7] W. Liu, J. Yang, B. Xiao, Application of Bayer red mud for iron recovery and building material production from alumosilicate residues, J. Hazard. Mater. 161 (2009) 474–478.
[8] Y. Liu, C. Lin, Y. Wu, Characterization of red mud derived from a combined Bayer process and bauxite calcination method, J. Hazard. Mater. 146 (2007) 255–261.
[9] N. Zhang, H. Sun, X. Liu, J. Zhang, Early-age characteristics of red mud-coal gangue cementitious material, J. Hazard. Mater. 167 (2009) 927–932.
[10] S.S. Amritphale, A. Anshul, N. Chandra, N. Ramakrishnan, A novel process for making radiopaque materials using bauxite-red mud, J. Eur. Ceram. Soc. 27 (2007) 1945–1951.
[11] I. Vangelatos, G.N. Angelopoulos, D. Boufounos, Utilization of ferroalumina as raw material in the production of Ordinary Portland Cement, J. Hazard. Mater. 168 (2009) 473–478.
[12] V.M. Sglavo, S. Maurina, A. Conci, A. Salviati, G. Carturan, G. Cocco, Bauxite 'red mud' in the ceramic industry. Part 2: production of clay-based ceramics, J. Eur. Ceram. Soc. 20 (2000) 245–252.
[13] T. Kavas, Use of boron waste as a fluxing agent in production of red mud brick, Build. Environ. 41 (2006) 1779–1783.
[14] J. Yang, D. Zhang, J. Hou, B. He, B. Xiao, Preparation of glass-ceramics from red mud in the aluminium industries, Ceram. Int. 34 (2008) 125–130.
[15] J. Somlai, V. Jobbagy, J. Kovacs, S. Tarjan, T. Kovacs, Radiological aspects of the usability of red mud as building material additive, J. Hazard. Mater. 150 (2008) 541–545.
[16] H. Liu, M.A. Abdou, R.J. Reed, A. Alice Ying, M.Z. Youssef, Neutronics assessment of the shielding and breeding requirements for FNSF (standard aspect ratio), Fusion Eng. Des. 85 (2010) 1296–1300.
[17] S.S. Amritphal, A. Anshul, N. Chandra, N. Ramakrishnan, Development of celsian ceramics from fly ash useful for X-ray radiation-shielding application, J. Eur. Ceram. Soc. 27 (2007) 4639–4647.
[18] X. Tian, B. Wu, J. Li, Method to prepare self-glazing ceramic materials using red mud and red sandstone, Chinese Patent 200710129576.8 (2008).
[19] E. Kamseu, C. Leonelli, D.N. Boccaccini, P. Veronesi, P. Miselli, G. Giancarlo, U. Chinje Melo, Characterisation of porcelain compositions using two china clays from Cameroon, Ceram. Int. 33 (2007) 851–857.
[20] B. Peterson. Egyptian Paste – An Ancient Form of Pottery. http://pottery.about.com/od/typesofclays/tp/Egyptian-Paste.htm.
[21] A.P. Merkin, M.I. Zeifman, M.A. Shenkao, Technology and properties of self-glazing ceramic tiles, Glass Ceram. 40 (1983) 513–516.
[22] J.A. Griggs, J.Y. Thompson, K.J. Anusavice, Effects of flaw size and auto-glaze treatment on porcelain strength, J. Dent. Res. 75 (1996) 1414–1417.
[23] X. Xiaorang Tian, B. Wu, J. Li, The exploration of making acid proof fracturing propants using red mud, J. Hazard. Mater. 160 (2008) 589–593.
[24] GB/T 3810.3-2006, Test methods of ceramic tiles – part 3: determination of water absorption, apparent porosity, apparent relative density and bulk density, China, 2006.
[25] QB/T 1548-1992, Test method for linear shrinkage of ceramic body, China, 1992.
[26] GB/T 4740-1999, Standard test method for compressive resistance of ceramic materials, China, 1999.
[27] GB 5101-2003, Fired common bricks, China, 2003.
[28] Guilin's Karst Landscape Formation, Guilin Karst Hills & Caves. http://www.chinaodysseytours.com/guilin/guilin-karst-hills-caves.html.
[29] J. Hakl, I. Hunyadi, I. Csige, G. Geczy, L. Lenart, A. Varhegyi, Radon transport phenomena studied in Karst caves-international experiences on radon levels and exposures, Radiat. Meas. 28 (1997) 675–684.
[30] J. Liu, J. Ye, H. Ying, J. Liu, M. Zheng, X. Gu, Sediment-hosted micro-disseminated gold mineralization constrained by basin paleo-topographic highs in the Youjiang basin, South China, J. Asian Earth Sci. 20 (2002) 517–533.
[31] G. Manic, S. Petrovic, M. Vesna, D. Popovic, D. Todorovic, Radon concentrations in a spa in Serbia, Environ. Int. 32 (2006) 533–537.
[32] B.A. Weaver, A.J. Westphal, Energy loss of relativistic heavy ions in matter, Nucl. Instrum. Methods B 187 (2002) 285–301.
[33] C. Domingo, Ll. Font, F. Fernandez, C. Baixeras, Identification of non-stopping ions with $Z > 65$ in polycarbonate track detector stacks, Radiat. Meas. 36 (2003) 281–285.